ISSN 1392–1320 MATERIALS SCIENCE (MEDŽIAGOTYRA). Vol. 24, No. 1. 2018

Thermal Stability and Decomposition Kinetics of AgO Submicron Particles Prepared by Potassium Persulfate Oxidation

Hui FENG [1], Wenning SHEN [2]*, Lajun FENG [2], Ali LEI [2], Yanfeng GE [2]

[1] *Shaanxi Institute of Zoology, No. 88 Xingqing Road, Xi'an 710032, China*
[2] *School of Materials Science and Engineering, Xi'an University of Technology, No. 5 South Jinhua Road, Xi'an 710048, China*

crossref http://dx.doi.org/10.5755/j01.ms.24.1.17052

Received 29 November 2017; accepted 17 July 2017

In this study, AgO submicron particles for antimicrobial application were prepared by potassium persulfate oxidation. The characterization of AgO particles was performed by XRD, XPS, SEM, TEM and TGA analysis. Its decomposition kinetics was studied by Doyle mechanism equation, Coats-Redfern equation and Ozawa approximate integration. The results showed that the as-prepared powders were composed of monoclinic AgO and small amounts of carbonate. The average width of AgO particles was about 200 nm with a rod-like morphology. AgO submicron particles could be decomposed to be Ag_2O at 123 °C. When the temperature was increased to 405 °C, Ag_2O was further transformed to be Ag. The decomposition reaction of AgO was controlled by Avrami-Erofeev random nucleation and subsequently growth mechanism (A1) with the apparent activation energy of 88.34 kJ/mol and the reaction frequency factor of 4.88×10^9 s^{-1}.
Keywords: AgO, TGA, thermal properties, thermodynamic properties.

1. INTRODUCTION

Silver containing compounds and materials have attracted considerable interests in recent years, since silver ions exhibit strong bacteriostatic and sterilization effects as well as a broad spectrum of antimicrobial activities [1 – 7]. The bacteria are difficult to resist silver containing products [8]. Furthermore, the antimicrobial property of different silver containing compounds and materials is relative to silver valence states, which the higher silver valence state has led to the better sterilization effect. So far the different materials have been studied, their effects are ordered in the following sequences: AgO > Ag_2O > Ag, $AgNO_3$ > Ag-ZSM-5 > Ag_2O > commercial silver-exchanged zeolite (granular) > commercial silver-exchanged zeolite (pellets) > Ag nanoparticles, respectively [9, 10]. The antimicrobial effect of silver dioxide has been extensively researched recently. Chen et al. [11] and Shen et al. [12] have reported that the antimicrobial effects of AgO are stronger than those of Ag_2O. Additionally, the materials in nano and submicro-size have special physical and chemical properties, such as antimicrobial property, because of their large ratio of surface area to volume and the high fraction of surface atoms [3, 13]. Thus, AgO submicron particles and nanoparticles might be important in the antimicrobial application; for instance, water treatment.

There are several methods to fabricate AgO particles, such as potassium persulfate oxidation [14, 15], ozone oxidation [12], chlorine oxidation [16], electrochemical process [17, 18], chemical bath deposition [19], etc. However, the thermal stability and decomposition kinetic of AgO bactericide vary depending on the reaction conditions, the preparation technology, the particle size and so on [20, 21]. Therefore, it is difficult to achieve the thermal stability law of AgO, which restricts its wide applications.

In our study, $AgNO_3$ and $K_2S_2O_8$ were used as precursors to prepare AgO submicron particles. Then the thermal stability of AgO submicron particles and their decomposition kinetics were determined by thermogravimetric analysis-differential thermal analysis (TGA-DTA) method. The present study is aimed to provide theoretical basis for the storage and application of AgO particles.

2. MATERIALS AND METHODS

2.1. Materials

$AgNO_3$ (≥ 99.8 % purity, Xi'an Nonferrous Metals Research Institute), $K_2S_2O_8$ and KOH (≥ 99.5 % and ≥ 85.0 % purity, Tianjin Tianli Chemical Reagent Co., Ltd.) were employed as reactants for the fabrication of AgO submicron particles. Deionized water was made in our laboratory.

2.2. Fabrication of AgO submicron particles

Potassium persulfate oxidation method was used to synthesize AgO submicron particles. The general procedures were as follows. 300 mL of $AgNO_3$ solution with a concentration of 0.05 mol/L was added into a 1000 mL three-necked flask. The $AgNO_3$ solution was then heated in a thermostat water bath at 60 ˚C. Subsequently, 200 mL of $K_2S_2O_8$ solution with a concentration of 0.225 mol/L was added drop-wisely into $AgNO_3$ solution under vigorous stirring. Later, 100 mL of KOH solution of 1.275 mol/L was slowly added into the mixture. The mixture was then mixing constantly for 20 min. After that, the solid product was obtained, followed repeatedly washing and drying at 50 °C for 6 h.

* Corresponding author. Tel.: +86-29-82312733; fax: +86-29-82312733.
E-mail address: *shenwenning@qq.com* (W. Shen)

2.3. Characterization

The prepared particles were characterized by an XRD-7000S X-ray diffractometer (XRD). XRD data were collected at a tube voltage of 40 kV, a tube current of 30 mA, 2 theta of 20 – 80°, and scan speed of 10°/min. The X-ray source was Cu X-ray with a λ of 0.15418 nm.

The element quantivalency of Element Ag and C was analyzed by X-ray photoelectron spectroscopy (XPS). The XPS spectra were achieved using a Kratos Axis Ultra instrument. The base pressure of the analytical chamber was 10^{-9} Torr. Spectra were excited using monochromatic AlKα (150 W, 15 kV, 1486.7 eV). The pass energy was 20 eV for narrow scanning. Binding energies were calibrated relative to the C1s peak (284.8 eV) from hydrocarbons adsorbed on the products' surface.

The morphology and particle size of the particles were examined by a JSM-6700F scanning electron microscope (SEM) and JEM-3010 transmission electron microscope (TEM). Before SEM analysis, the sample was covered with Pt thin film. The micrographs were obtained at an accelerating voltage of 20 kV and an accelerating current of 10 μA.

Thermal stability of the product was analyzed by WRT-3P trace thermobalance, using air as measuring atmosphere. The heating rates were 5°C/min, 10°C/min, 15°C/min and 20°C/min respectively. Its corresponding tested sample amounts were 32.92 mg, 40.42 mg, 32.5 mg and 32.67 mg respectively.

3. RESULTS AND DISCUSSION

3.1. Analysis of AgO submicron particles

Fig. 1 shows the XRD pattern of AgO particles. All diffraction peaks observed in the obtained XRD pattern (marked with '▼') corresponded to monoclinic structure of AgO (JCPDS card#89-3081). This indicated that AgO with a crystal structure of monoclinic system was successfully obtained.

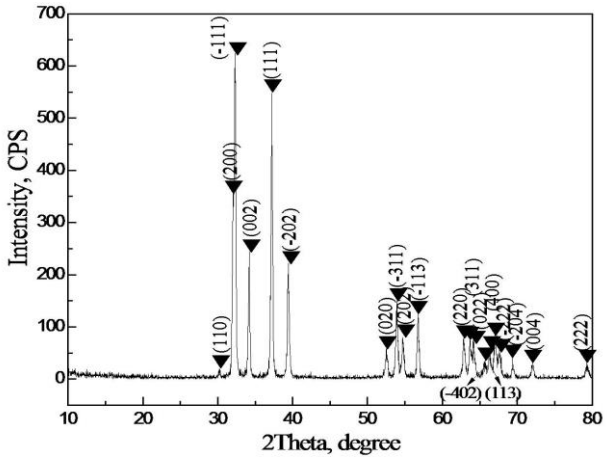

Fig. 1. XRD pattern of obtained AgO particles

Fig. 2 shows the XPS results of the particles. The silver electronic state in the particles can be derived from the high-resolution XPS spectrum. The core-level Ag 3d spectrum for the particles was broad, the asymmetric peaks at 374.1 eV and 368.0 eV, which were easily appointed to core-level $Ag3d_{3/2}$ and $Ag3d_{5/2}$ photoemissions, respectively.

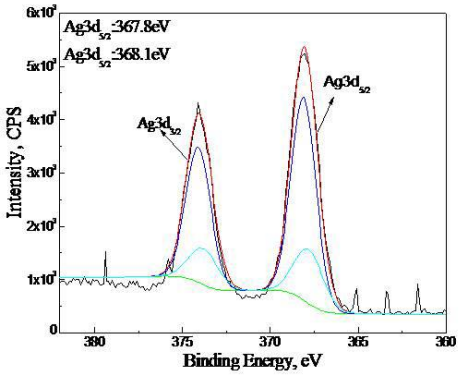

Fig. 2. XPS Ag3d spectrum for obtained AgO particles

The high-resolution $Ag3d_{5/2}$ spectrum was decomposed into two individual component peaks. This indicated that the element silver in the particles was in two forms. The peak at 368.1 eV corresponded to AgO [22], while the peak at 367.7 eV was carbonate containing silver. Spectroscopic evidence for surface carbonate species was detected in the O1s and C1s spectra (O1s = 531.5 eV, C1s = 288.7 eV, Fig. 3).

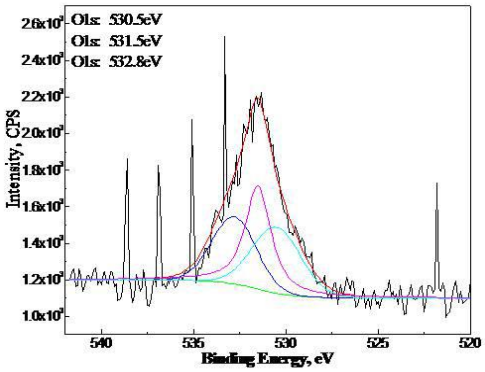

a

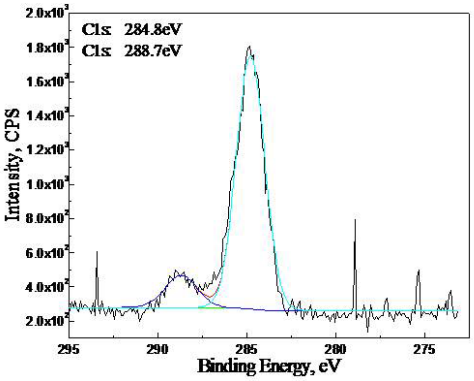

b

Fig. 3. XPS spectra for obtained AgO particles: a – of O1s; b – C1s

In addition, the peak at 532.8 eV was from the hydroxyl or adsorbed water on the surface of AgO powders. The formation of carbonate was from the reaction of surface oxygen atoms with atmospheric CO_2, which was a distinguishing feature common to all silver oxide [18].

This result showed that the particles were composed of AgO and small amounts of carbonate. Since carbonate was just formed on the surface of AgO, its content was too small to be detected by XRD.

Fig. 4 shows the SEM image and TEM micrograph of AgO particles. It can be seen that, the particle has a flake-like morphology. The average width and length of the particles are about 200 nm and 500 nm, respectively.

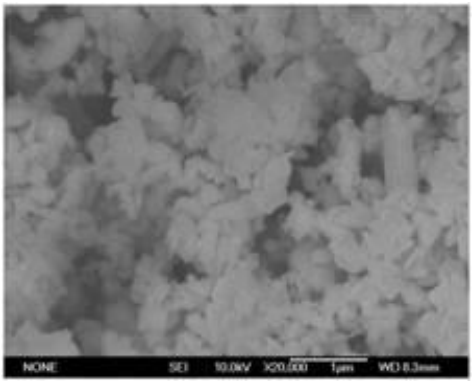

a

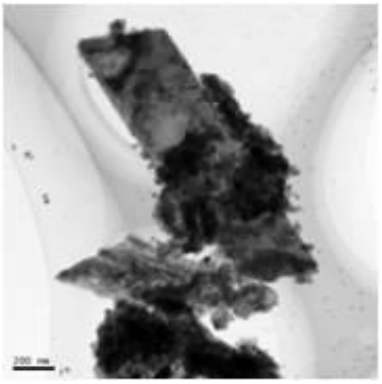

b

Fig. 4. a – SEM image; b – TEM micrograph of obtained AgO particles

3.2. Thermal stability analysis of AgO submicron particles

Fig. 5 shows the results of TGA for the AgO submicron particles.

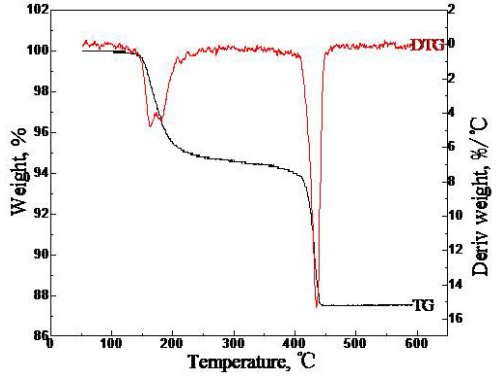

Fig. 5. TGA-DTA curves of obtained AgO particles at a heating rate of 15 °C/min

Two peaks of weight loss in the dynamic TGA curve were observed in the whole temperature programming process. AgO was decomposed in two steps. The first peak in the TGA curve was located between 123 °C and 226 °C. The weight loss percentage was about 6.18 %. Since AgO can be decomposed into Ag_2O and release O_2, which is represented as follows

$$4AgO = 2Ag_2O + O_2 \uparrow . \quad (1)$$

According to Eq. 1, the theoretical weight loss was calculated to be 6.46 %, which was consistent with theoretical value. AgO was decomposed into Ag_2O. The second stage of weight loss was in the range of 413 ~ 452 °C. It could be resulted from the decomposition of Ag_2O into Ag. Its thermo-gravimeteric loss percentage is 6.995 %. The decomposition of Ag_2O is expressed as follows:

$$2Ag_2O = 4Ag + O_2 \uparrow . \quad (2)$$

The theoretical mass loss caused by O_2 release is 6.9 %, which accords with experimental loss value. It confirmed the hypothesis of the decomposition of Ag_2O into Ag. Thus, as a bactericide for water treatment, AgO particles must be used and store in temperature lower than 100 °C.

3.3. Decomposition kinetic analysis of AgO decomposition

Based on non-isothermal reaction kinetics theory [23], under linear temperature increase condition, the kinetic equation for the decomposition of solid matter is represented as:

$$\beta \cdot \frac{d\alpha}{dT} = A \cdot e^{-\frac{E}{RT}} \cdot f(\alpha), \quad (3)$$

where α is the decomposition fraction at temperature T, $f(\alpha)$ the mechanism function of decomposition kinetics, A the frequency factor (s^{-1}), E the activation energy (J/mol), T the temperature for decomposition reaction, and β the linear heating rate (°C/min).

The non-isothermal kinetics of thermal decomposition of AgO into Ag_2O was studied using single TG curve. Firstly, Doyle mechanism equation was adopted, which is shown as follows [24, 25]:

$$\ln F(\alpha) = \ln \frac{AE}{\beta R} - 5.3305 - 1.052 \frac{E}{R} \cdot \frac{1}{T}, \quad (4)$$

where,

$$F(\alpha) = \int_0^{\alpha} \frac{d\alpha}{f(\alpha)} \cdot$$

As shown in Eq. 4, there is a linear relationship between the $\ln F(\alpha)$ and $(1/T)$. Ten functions of most commonly used mechanisms of solid state process (Table 1) [25] were separately substituted into equation 4, and the linear correlation coefficient (r) was obtained by least square method. Meanwhile, the activation energy (E) and reaction frequency factor (A) were calculated from the slope and intercept of straight line respectively.

To compare the results above, Coats-Redfern equation (Eq. 5) was used to estimate the kinetic parameters [24].

$$\ln \frac{F(\alpha)}{T^2} = \ln[\frac{AR}{E\beta}(1 - \frac{2RT}{E})] - \frac{E}{R} \cdot \frac{1}{T} . \quad (5)$$

Table 1. Most frequently used mechanisms of solid state process

Mechanism	Symbol	*f(α)*	*F(α)*
1 – dimensional diffusion	D1	$0.5/\alpha$	α^2
2 – dimensional diffusion (Valensi eqution)	D2	$[-\ln(1-\alpha)]^{-1}$	$\alpha+(1-\alpha)\ln(1-\alpha)$
3 – dimensional diffusion (sphere. Jander equation)	D3	$1.5(1-\alpha)^{2/3}[1-(1-\alpha)^{1/3}]^{-1}$	$[1-(1-\alpha)^{1/3}]^2$
3 – dimensional diffusion (cylinder, G – B equation)	D4	$1.5[(1-\alpha)^{-1/3}-1]^{-1}$	$(1-2\alpha/3)-(1-\alpha)^{2/3}$
2 – dimensional phase boundary reaction	R2	$2(1-\alpha)^{1/2}$	$1-(1-\alpha)^{1/2}$
3 – dimensional phase boundary reaction	R3	$3(1-\alpha)^{2/3}$	$1-(1-\alpha)^{1/3}$
Nucleation and nuclei growth (Avrami-Erofeev equation, n = 1)	A1	$1-\alpha$	$-\ln(1-\alpha)$
Nucleation and nuclei growth (Avrami-Erofeev equation, n = 1.5)	A1.5	$1.5(1-\alpha)[-\ln(1-\alpha)]^{1/3}$	$[-\ln(1-\alpha)]^{2/3}$
Nucleation and nuclei growth (Avrami-Erofeev equation, n = 2)	A2	$2(1-\alpha)[-\ln(1-\alpha)]^{1/2}$	$[-\ln(1-\alpha)]^{1/2}$
Nucleation and nuclei growth (Avrami-Erofeev equation, n = 3)	A3	$3(1-\alpha)[-\ln(1-\alpha)]^{2/3}$	$[-\ln(1-\alpha)]^{1/3}$

If the value of $(2RT/E)$ changes a little bit with the temperature, it can be considered as constant in temperature programming process. Then $\ln(F(\alpha)/T^2)$ is a linear function for $(1/T)$. Ten functions of most frequently used mechanisms of solid state process (Table 1) were separately substituted into Eq. 5, and the linear correlation coefficient (r) was obtained by least square method. Subsequently, the activation energy was calculated from the straight line slope, and the frequency factor was obtained from the intercept at the mean temperature of decomposition.

It is reasonable to directly obtain the kinetic parameters of the thermal decomposition from the experimental data of α and T by adopting above two integration methods, since they can avoid the error introduced by the calculation of $d\alpha/dT$. The experimental data of α and corresponding T for the decomposition of AgO into Ag_2O heated at heating rate of 15 °C/min are shown in Fig. 6. Using Doyle mechanism equation and Coats-Redfern equation, the data in Fig. 6 were separately substituted into Eq. 4 and Eq. 5, and the results are shown in Table 2 and Table 3 respectively.

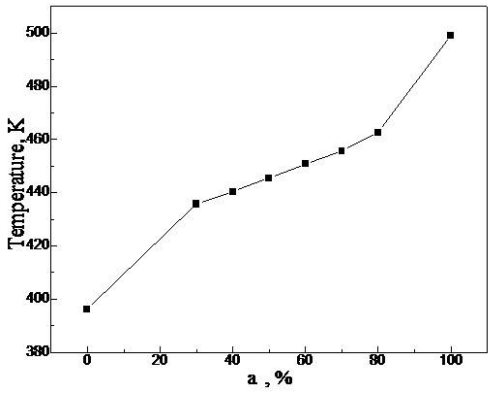

Fig. 6. T versus α in the decomposition of obtained AgO at a heating rate of 15 °C/min

In general, the linear correlation was used to determine the decomposition mechanism. If the mechanism function ($F(\alpha)$) might reflect the real situation of decomposition accurately, the linear correlation was better. As shown in Table 2 and Table 3, the results from Doyle mechanism equation and Coats-Redfern equation are not quite different. Among the fitting results, the maximum value of linear correlation coefficient is 0.99095 and the minimum value of standard deviation is 0.0012, corresponding to the mechanism of nucleation and nuclei growth (Avrami-Erofeev equation, n = 1; Al). Thus, the decomposition reaction of AgO submicron particles prepared by potassium persulfate oxidation obeys A1 mechanism.

Table 2. Fitted results of solid state reaction mechanisms for decomposition of AgO from Doyle equation

Mechanism	*E*, kJ/mol	*A*, s^{-1}	*r*, a.u.	*s*, a.u.
D1	114.587	2.19×10^{12}	0.95912	0.0873
D2	131.757	1.55×10^{14}	0.97169	0.0791
D3	153.406	1.75×10^{16}	0.98343	0.0622
D4	138.897	2.68×10^{14}	0.97626	0.0734
R2	71.386	2.06×10^{7}	0.97854	0.0175
R3	76.703	6.14×10^{7}	0.98343	0.0012
A1	88.343	4.88×10^{9}	0.99095	0.0012
A1.5	58.869	1.96×10^{6}	0.99095	0.0050
A2	44.152	4.27×10^{4}	0.99095	0.0028
A3	29.434	1.05×10^{3}	0.99095	0.0155

Table 3. Fitted results of solid state reaction mechanisms for decomposition of AgO from Coats-Redfern method

Mechanism	*E*, kJ/mol	*A*, s^{-1}	*r*, a.u.	*s*, a.u.
D1	113.08	1.43×10^{12}	0.95349	0.0878
D2	131.15	1.33×10^{14}	0.96827	0.0796
D3	153.92	2.05×10^{16}	0.98168	0.0626
D4	138.66	2.57×10^{14}	0.97353	0.0739
R2	67.635	5.26×10^{6}	0.97331	0.0177
R3	73.229	1.81×10^{7}	0.97966	0.0158
A1	85.432	1.90×10^{9}	0.98915	0.0114
A1.5	54.467	3.42×10^{5}	0.98805	0.0051
A2	38.985	4.27×10^{3}	0.98680	0.0029
A3	23.502	49.916	0.98364	0.0013

Based on the determined function model of A1 mechanism, the decomposition kinetic parameters of AgO particles were calculated by employing Doyle mechanism equation, which has better linear correlation. The obtained apparent activation energy and the reaction frequency factor were 88.34 kJ/mol and 4.88×10^9 s^{-1} respectively. For the obtained activation energy, the value of (E/RT) was in the range of 21.17 ~ 26.88 at the decomposition temperature, agreeing with the assumption of $20 \le (E/RT) \le 60$ for Doyle mechanism equation. This proved that the use of Doyle mechanism equation to study the decomposition kinetics of AgO was reasonable. The dynamical equation for the decomposition of AgO into Ag_2O is as follows:

$$-\frac{d\alpha}{dt} = 4.88\times10^{9} \times e^{-\frac{88.34\times10^{3}}{RT}} \times (1-\alpha) \cdot \qquad (6)$$

To further confirm the rationality of the determined A1

mechanism, Ozawa approximate integration was employed to calculate the decomposition kinetic parameters of AgO. The calculation of activation energy by Ozawa approximate integration does not involve the selection of mechanism functions, avoiding the error caused by choosing decomposition mechanism.

Ozawa equation [26]:

$$\lg \beta = \lg \frac{AE}{RG(\alpha)} - 2.315 - 0.4567 \frac{E}{RT}, \quad (7)$$

where

$$G(\alpha) = \int_0^{\alpha} \frac{d\alpha}{f(\alpha)} = \frac{A}{\beta} \int_0^{T} e^{-\frac{E}{RT}} dT \cdot$$

Since the value of $G(\alpha)$ changes very little with the temperature, it can be regarded as constant during temperature programming. Thus, there has a linear relationship between lgβ and (1/T) at different decomposition fraction. The straight slope can be obtained by linear fitting. Subsequently, the apparent activation energy at different decomposition fraction can be derived from the slope.

AgO submicron particles were separately heated at the rate of 5, 10, 15, 20 °C/min to obtain the TG curves. Based on the TG curves, different decomposition fraction and its corresponding temperature are shown in Fig. 7. At the same decomposition fraction, the values of lgβ and T in Fig. 7 were substituted into equation, and the results are shown in Table 4.

Table 4. Activation energy of AgO decomposition obtained from Ozawa method under different α

α	30 %	40 %	50 %	60 %	70 %	80 %
E, kJ/mol	87.53	82.64	84.42	82.53	86.54	84.38
r, a.u.	0.99455	0.99297	0.98061	0.98617	0.98894	0.95025

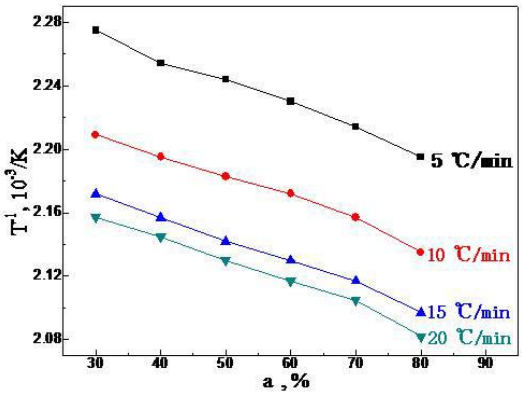

Fig. 7. T versus α in the decomposition of obtained AgO at different heating rate

Among the apparent activation energy in Table 2, Table 3 and Table 4, only the activation energy derived from A1 mechanism better matches those for different decomposition fraction. This indicated the validity of A1 mechanism was obtained from Doyle equation and Coats-Redfern equation. Thus, the decomposition of AgO particles prepared by potassium persulfate oxidation was a process in which the nucleation and subsequent growth take place concurrently. Since heat from outside environment was adsorbed, the temperature of the lattice points in a monoclinic lattice increased. The increase of temperature intensified the vibration of the lattice points, leading to the formation of local reaction center which caused the decomposition of AgO. Subsequently, the silver oxide phase nucleated, and the dispersed crystal nucleus grew simultaneously, accelerating the decomposition of AgO crystal. In other words, the whole decomposition of AgO was a process in which the monoclinic structure of AgO was destroyed by the breaking of Ag-O-Ag chemical bonds and the ultimate phase of Ag_2O was formed.

4. CONCLUSIONS

High crystallized AgO submicron particles with a rod-like shape were fabricated by chemical precipitation method using $K_2S_2O_8$ as oxidation in the present study. AgO submicron particles were decomposed to be Ag_2O at 123 °C. When the temperature was increased to 405 °C, Ag_2O was further transformed to be Ag. This suggested that AgO submicron particles were unstable up to the temperature of 123 °C. The decomposition reaction of AgO obeyed random nucleation and subsequent nuclei growth mechanism (Avrami-Erofeev equation, n=1) with an apparent activation energy of 88.34 kJ/mol and a reaction frequency factor of 4.88×10^9 s^{-1}. The corresponding kinetic equation of AgO decomposition is expressed as

$$-\frac{d\alpha}{dt} = 4.88 \times 10^9 \times e^{-\frac{88.34 \times 10^3}{RT}} \times (1-\alpha) \cdot \quad (8)$$

Based on the obtained results, it can be concluded that AgO submicron particles prepared by potassium persulfate oxidation should be stored and employed under 120 °C to play the best bactericidal effect.

Acknowledgments

This work was supported financially by Key Project of Agricultural Science and Technology Innovation of Shaanxi Province (2015NY060), Key Laboratory Project of Education Department of Shaanxi Province (No. 15JS080), Key Programe-Scientific Research Project of Education Department of Shaanxi Province for 2018, Science and Technology Co-ordination & Innovation Key Laboratory Project of Shaanxi Province (2014SZS09-Z02) and Program of Shaanxi Academy of Sciences (2016K-24).

REFERENCES

1. **Mirzajani, F., Ghassempour, A., Aliahmadi, A., Esmaeili, M.A.** Antibacterial Effect of Silver Nanoparticles on Staphylococcus Aureus *Research in Microbiology* 16 2011: pp. 542 – 549. https://doi.org/10.1016/j.resmic.2011.04.009
2. **Panacek, A., Kolar, M., Vecerova, R., Prucek, R., Soukupova, J., Krystof, V., Hamal, P., Zboril, R., Kvitek, L.** Antifungal Activity of Silver Nanoparticles against Candida spp *Biomaterials* 30 2009: pp. 6333 – 6340. https://doi.org/10.1016/j.biomaterials.2009.07.065

3. **Martinez-Gutierrez, F., Olive, P.L., Banuelos, A., Orrantia, E., Nino, N., Sanchez, E.M., Ruiz, F., Bach, H., Av-Gay, Y.** Synthesis, Characterization, and Evaluation of Antimicrobial and Cytotoxic Effect of Silver and Titanium Nanoparticles *Nanomedicine, Nanotechnology, Biology, and Medicine* 6 2010: pp. 681 – 688. https://doi.org/10.1016/j.nano.2010.02.001
4. **Hernandez-Sierra, J.F., Ruiz, F., Pena, D.C.C., Martinez-Gutierrez, F., Martinez, A.E., Guillen, A. de J.P., Tapia-Perez, H., Castanon, G.M.** The Antimicrobial Sensitivity of Streptococcus Mutans to Nanoparticles of Silver, Zinc Oxide, and Gold *Nanomedicine, Nanotechnology, Biology, and Medicine* 4 2008: pp. 237 – 240. https://doi.org/10.1016/j.nano.2008.04.005
5. **Gangadharan, D., Harshvardan, K., Gnanasekar, G., Dixit, D., Popat, K.M., Anand, P.S.** Polymeric Microspheres Containing Silver Nanoparticles as a Bactericidal Agent for Water Disinfection *Water Research* 44 2010: pp. 5481 – 5487. https://doi.org/10.1016/j.watres.2010.06.057
6. **Shen, W., Feng, L., Feng, H., Kong, Z., Guo, M.** Ultrafine Silver (II) Oxide Particles Decorated Porous Ceramic Composites for Water Treatment *Chemical Engineering Journal* 175 2011: pp. 592 – 599. https://doi.org/10.1016/j.cej.2011.09.121
7. **Shen, W., Feng, L., Feng, H., Lei, A.** Divalent Silver Oxide-Diatomite Hybrids: Synthesis, Characterization and Antibacterial Activity *Ceramics International* 39 2013: pp. 5013 – 5024. https://doi.org/10.1016/j.ceramint.2012.11.099
8. **Rai, M., Yadav, A., Gade, A.** Silver Nanoparticles as a New Generation of Antimicrobials *Biotechnology Advances* 27 2009: pp. 76 – 83. https://doi.org/10.1016/j.biotechadv.2008.09.002
9. **Yang, H., Wang, K., Ding, X., Zhou, G., Ge, M.** Study on Relationship between Antibacterial Property and Silver Ions in Inorganic Antibacterial Powders *Journal of Chinese Ceramics Society* 30 2002: pp. 585 – 588 (in Chinese).
10. **Lalueza, P., Monzon, M., Arruebo, M., Santamaria, J.** Bactericidal Effects of Different Silver-containing Materials *Materials Research Bulletin* 46 2011: pp. 270 – 2076. https://doi.org/10.1016/j.materresbull.2011.06.041
11. **Chen, K., Li, Q., Jiao, L., Zhou, G.** Preparation of Nano-divalent Silver Powder and its Sterilization Properties *Journal of East China University of Science and Technology (Natural Science Edition)* 34 2008: pp. 86 – 90.
12. **Shen, W., Feng, L., Kong, Z., Feng, H.** Ultrafine Silver Peroxide Powders Prepared by Ozone Oxidization Method and its Antibacterial Property *Acta Chimica Sinica* 69 2011: pp. 277 – 283 (in Chinese).
13. **Shahverdi, A.R., Fakhimi, A., Shahverdi, H.R., Minaian, S.** Synthesis and Effect of Silver Nanoparticles on the Antibacterial Activity of Different Antibiotics against Staphylococcus aureus and Escherichia coli *Nanomedicine: Nanotechnology Biology and Medicine* 3 2007: pp. 168 – 171. https://doi.org/10.1016/j.nano.2007.02.001
14. **Li, Q., Chen, K., Jiao, L., Zhou, G.** The Preparation of the Dispersed Liquid of Nanometer Bivalent Silver Oxide *Water Purification Technology* 27 2008: pp. 12 – 15 (in Chinese).
15. **Shen, W., Feng, L., Lei, A., Kong. Z.** Preparation of Ultra Silver Peroxide Powder and Characterization *Rare Metal Materials and Engineering* 40 2011: pp. 31 – 35 (in Chinese).
16. **Zhang, Y.** The Synthesis of Nano-AgO and its Electrochemical Performance. M.S. Thesis, Beijing University of Chemical Technology, Beijing, 2007 (in Chinese).
17. **Jordan, M.B., Feng, Y., Burkett, S.L.** Development of Seed Layer for Electrodeposition of Copper on Carbon Nanotube Bundles *Journal of Vacuum Science & Technology B* 33 2015: pp. 021202. https://doi.org/10.1116/1.4907164
18. **Waterhouse, G.I.N., Metson, J.B., Bowmaker, G.A.** Synthesis, Vibrational Spectra and Thermal Stability of Ag_3O_4 and Related Ag_7O_8X Salts ($X=NO_3^-, ClO_4^-, HSO_4^-$) *Polyhedron* 26 2007: pp. 3310 – 3322. https://doi.org/10.1016/j.poly.2007.03.006
19. **Kocareva, T., Grozdanov, I., Pejova, B.** Ag ang AgO Thin Film Formation in Ag^+ — Triethanolamine Solutions *Materials Letters* 47 2001: pp. 319 – 323. https://doi.org/10.1016/S0167-577X(00)00257-3
20. **Yue, L., Shui, M., Xu, Z.** The Crystal Structure of Ultra-fine $CaCO_3$ and its Thermal Decomposition *Chemical Journal of Chinese Universities* 21 2000: pp. 1555 – 1559 (in Chinese).
21. **Smith, D.F., Brown, C.** Aging in Chemically Prepared Divalent Silver Oxide Electrodes for Silver/zinc Reserve Batteries *Journal of Power Sources* 96 2001: pp. 121 – 127. https://doi.org/10.1016/S0378-7753(00)00679-0
22. **Gerenser, L.J.** Photoemission Investigation of Silver/poly-(ethylene terephthalate) Interfacial Chemistry: the Effect of Oxygen-plasma Treatment *Journal Vacuum Science & Technology A* 8 1990: pp. 3682 – 3691. http://dx.doi.org/10.1116/1.576480
23. **Hu, R., Shi, Q.** Thermal Analysis Kinetics. Science Press, Beijing, 2001: pp. 230 – 238 (in Chinese).
24. **Li, F., He, J., Du, Y., Evans, D.G., Wang, Z., Duan, X.** Study on the Preparation and Non-isothermal Kinetics of Thermal Decomposition of α-zirconium Phosphate *Journal of Inorganic Chemistry* 15 1999: pp. 55 – 60 (in Chinese).
25. **Chu, S.** Thermal Analysis of Explosives. Science Press, Beijing, 1994: pp. 159 – 165 (in Chinese).
26. **Li, Q., Chen, S., Yao, P., Wei, G., Qu, Y.** Thermal Decomposition Mechanism of the Nano-$BaTiO_3$ Formation *Acta Physico-Chimica Sinica* 16 2000: pp. 170 – 174 (in Chinese).